International Journal of
Drug Discovery and Pharmacology（IJDDP）

Scilight

Article

Ginsenoside Re Alleviates Oxidative Stress Damage and Ferroptosis in Pulmonary Fibrosis Mice by Regulating the Nrf2/Keap1/GPX4 axis

Huicai Lin [1,2,3], Zhaoqin Wen [1,2,3], Linying Feng [1,2,3], Xiaoyan Chen [4], Yongxiang Song [5], and Jiang Deng [1,2,3,*]

[1] Key Laboratory of Basic Pharmacology of Ministry of Education and Joint International Research Laboratory of Ethnomedicine of Ministry of Education, Zunyi Medical University, Zunyi563006, China
[2] Key Laboratory of Basic Pharmacology of Guizhou Province, Zunyi Medical University, Zunyi563006, China
[3] The Second Affiliated Hospital of Zunyi Medical University, Zunyi Medical University, Zunyi563006, China
[4] Department of Pathophysiology, Zunyi Medical University, Zunyi563006, China
[5] Department of Thoracic Surgery, Affiliated Hospital of Zunyi Medical University, Zunyi563006, China
* Correspondence: dengjiang1225@zmu.edu.cn; Tel.: +86-851-2864-3411; Fax: +86-851-2864-3411

Received: 30 August 2024; Revised: 28 September 2024; Accepted: 30 September 2024; Published: 17 December 2024

Abstract: Pulmonary fibrosis (PF) is a chronic, progressive, irreversible, fibrotic interstitial lung disease with high mortality. Ginsenoside Re (G-Re) is one of the active components of ginseng, which has been proven to possess multiple pharmacological effects, including anti-inflammatory and antioxidant. Thus, G-Re is considered a potential therapeutic agent for treating PF. The present study explored the protective mechanisms of G-Re against bleomycin (BLM) -induced PF in mice and its potential as a therapeutic strategy for PF. A mouse model of BLM-induced PF was utilized to assess the effect of G-Re treatment, with N-acetylcysteine (NAC) set as a positive control agent. Various parameters such as lung function, histopathological changes, oxidative stress markers, nuclear factor erythroid 2-related factor 2 (Nrf2) nuclear translocation and its related protein expressions, including Kelch-like ECH-associated protein 1 (Keap1), heme oxygenase 1 (HO-1), and NAD(P)H quinone oxidoreductase 1 (NQO-1), and ferroptosis signature protein glutathione peroxidase 4 (GPX4) were evaluated. Continuous administration of G-Re for 14 days significantly reduced lung injury, enhanced antioxidant capacity, activated the Nrf2/Keap1 signaling pathway, and inhibited ferroptosis as evidenced by GPX4. Additionally, G-Re treatment reduced collagen deposition, improved pulmonary function, and alleviated oxidative stress in the lung tissue of PF mice. These findings demonstrate that G-Re exerts its therapeutic effects against PF by modulating the Nrf2/Keap1/GPX4 axis and targeting oxidative stress and ferroptosis pathways, highlighting the potential of G-Re as a pharmacological intervention for PF and providing insights into the molecular mechanisms underlying its protective effects.

Keywords: pulmonary fibrosis; ginsenoside Re; oxidative stress; ferroptosis; Nrf2; GPX4

1. Introduction

Pulmonary fibrosis (PF) is a progressive, irreversible, and age-associated chronic interstitial lung disease with high morbidity and mortality [1]. The pathological features of PF encompass abnormal interstitial hyperplasia, excessive collagen deposition, and sustained injury to alveolar epithelial cells. These changes result in the formation of extensive fibrous cicatricial tissue, leading to diminished lung compliance and, in severe instances, culminating in pulmonary failure [2]. PF is triggered by various factors, including environmental exposure, chemotherapy, radiation, severe infection, or idiopathic PF. The median survival

duration of patients after diagnosis is approximately 3–5 years [3]. Although nintedanib and pirfenidone are the two medications approved for PF treatment, they are ineffective at improving the survival rate or quality of life of patients. Moreover, nintedanib and pirfenidone have been associated with notable adverse drug reactions affecting the gastrointestinal tract, nervous system, and dermal tissues. The exorbitant cost has also proven to be a deterrent for most patients [4, 5]. Thus, identifying alternative pharmacotherapeutic agents characterized by reduced adverse effects and a more economically viable cost structure for patients with PF is paramount.

Although numerous studies on PF have been investigated, the underlying molecular mechanisms of PF are yet to be fully understood. Accumulating evidence suggests that oxidative stress injury plays a crucial role in the physiological and pathological processes of PF [6,7]. Oxidative stress injury involves the accumulation of reactive oxygen species (ROS), including reactive nitrogen species (RNS), singlet oxygen (O^2), superoxide anion ($O^{2\bullet-}$), hydrogen peroxide (H_2O_2), nitric oxide (NO•), hydroxyl radical (OH•), and hydroxyl ion (OH^-), leading to an imbalance between endogenous oxidation and antioxidant systems, which results in lipid peroxidation of the cell membrane, protein oxidative modification, and DNA damage [8, 9]. Notably, the nuclear factor erythroid 2 related factor 2 (Nrf2) and its specific repressor, kelch-like ECH-associated protein 1 (Keap1), serve as a crucial cellular defense mechanism against oxidative stress injury [10]. The Nrf2/Keap1 signaling pathway regulates a series of cytoprotective genes, including superoxide dismutase (SOD), NAD(P)H quinone oxidoreductase-1 (NQO-1), heme oxygenase-1 (HO-1), and glutathione peroxidase 4 (GPX4), promoting the production of reduced glutathione (GSH) [11]. Moreover, oxidative stress leads to the intracellular accumulation of phospholipid hydroperoxides, which react with both ferrous and ferric ions, causing rapid and irreversible damage to cell membranes, ultimately resulting in cell death. This series of cascading events is known as the Fenton reaction and serves as a hallmark of cellular ferroptosis [12]. As a crucial neutralizing enzyme in this process, GPX4 catalyzes the conversion of two molecules of GSH into oxidized glutathione, thereby reducing toxic phospholipid hydroperoxides to non-toxic products, and plays a crucial role in suppressing cellular ferroptosis [13, 14]. Prior investigations have documented the protective effect of the Nrf2/Keap1 signaling pathway on pulmonary injury, attributed to the increased expression of GPX4 and subsequent inhibition of ferroptosis [15, 16]. However, the activation status of the Nrf2/Keap1/GPX4 axis in PF remains unclear. Consequently, targeting and inhibiting the Nrf2/Keap1/GPX4 axis emerges as a potentially promising therapeutic strategy for PF, given its potential role in modulating oxidative stress and ferroptosis pathways.

Ginseng (*Panax ginseng C.A. Mey*), a perennial herb belonging to the Araliaceae family, has been used as a tonic medicine in traditional Chinese medicine for over 2000 years. The pharmacological effects of ginseng have been demonstrated in metabolism, infectious diseases, tumors, and central nervous system disorders [17]. Moreover, within the spectrum of active compounds in ginseng, ginsenoside Re (G-Re), a protopanaxatriol-ginsenoside, stands out as a crucial component with notable pharmacological properties. Numerous studies have elucidated the multifaceted pharmacological effects of G-Re, including antioxidant, anti-inflammatory, antiviral, anti-cancer, and neuroregulatory properties [18-20]. Furthermore, our previous investigation revealed a discernible protective effect of G-Re against bleomycin (BLM)-induced PF in mice. However, the precise molecular mechanism underlying this effect remains elusive. Building upon our prior research and integrating insights from existing literature, the current study sought to delve deeper into the interplay between the anti-PF properties of G-Re, Nrf2/Keap1 signaling pathway, and ferroptosis. This study seeks to furnish scientific evidence supporting the therapeutic potential of G-Re in treating PF.

2. Materials and Methods

2.1. Regents

G-Re (high-performance liquid chromatography (HPLC) ⩾ 95%) (Cat#20200601) was procured from Hengkang Yibai Technology Co., Ltd. (Beijing, China). BLM (Cat#20067411) was obtained from Hanhui Pharmaceutical Co., Ltd. (Shanghai, China). N-acetylcysteine (NAC) (Cat#IA0050), Sirius Red dye (Cat# 1471), and improved Masson's trichrome staining solution (Cat#1346) was sourced from Solarbio Technology Co., Ltd. (Beijing, China). Myeloperoxidase (MPO) (Cat#E-BC-K074-M), malondialdehyde (MDA) (Cat#E-BC-K025-M), total antioxidant capacity (T-AOC) (Cat#E-BC-K136-M), T-SOD (Cat#E-BC-

K020-M), and GSH (Cat#E-BC-K030-M) colorimetric test kits were was from Elabscience Biotechnology Co., Ltd. (Wuhan, China). Keap1 (Cat#ab119403), HO-1(Cat#ab68477), and GPX4 (Cat#ab125066) antibodies were acquired from Abcam (Cambridge, MA, USA). Alpha-smooth muscle actin (α-SMA) (Cat# 55135-1-AP), β -actin (Cat#6609-I-Ig), Alexa Flour 488 Labeled Goat Anti-Mouse IgG (H + L) (Cat#SA00013-1), Alexa Flour 488 Labeled Goat Anti-IgG (H + L) (Cat#SA000), Alexa Flour 594 Labeled Goat Anti-Rabbit IgG (H + L) (Cat#SA00013-4), horseradish peroxidase (HRP)-conjugated Affinipure Goat Anti-Mouse IgG (Cat#AB-92455), and HRP-conjugated Affinipure Goat Anti-Rabbit IgG (Cat#AB-10122492) were procured from Proteintech Group Inc. (Rosemont, IL, USA).

2.2. Animals

Forty male C57BL/6J mice (8 – 12 weeks old, 18 – 22 g body weight) were obtained from SPF Biotechnology Co., Ltd. (Beijing, China, certificate No. SCXK 2019-0010). Mice were accommodated in a specific pathogen-free facility under controlled environmental conditions, including a room temperature of 22 – 26 °C, relative humidity of 55 ± 5%, and a 12: 12-h dark-light cycle. All experimental protocols were approved by the Ethics Committee of Zunyi Medical University (approval No. ZMU21-2203-583). The experimental procedures strictly adhered to the guidelines established in the US National Institutes of Health guide for the care and use of laboratory animals (National Institutes of Health Publication 85-23, revised 1996).

2.3. Experimental Model for PF

After one week of adaptive feeding, the experiment was carried out on a BLM-induced PF mouse model as previously described [10]. Briefly, mice were anesthetized by intraperitoneal injection of 2% pentobarbital sodium until unconscious and then fixed to a mouse plate in a supine position. The trachea was exposed through a midline incision in the neck, through which BLM was injected into the trachea between the cartilage rings of the trachea. Following the injection, mice were positioned upright and rotated at a constant speed along the longitudinal axis for 3 min to ensure even distribution of BLM (3 mg/kg) in both lungs. In addition, mice in the Sham group received an equivalent dose of saline as a control. Subsequently, mice were sterilized, sutured, and intramuscularly injected with 120,000 U of benzathine penicillin to prevent postoperative infections.

2.4. Experimental Treatment Protocols

NAC is a widely utilized therapeutic agent in respiratory medicine, demonstrating efficacy in conditions such as bronchiectasis, influenza, and idiopathic PF. Consequently, NAC was employed as a positive control in this study [21]. The surviving PF mice were randomly divided into three groups in a 1: 1 ratio: Model group, Model + G-Re group, and Model + NAC group. Mice in Model + G-Re and Model + NAC groups received G-Re 10 mg/kg or NAC respectively by gavage from days 2 – 14. Mice in the Sham and Model groups received an equivalent volume of saline.

2.5. Assessment of Pulmonary Function and Index

After 1 h of the final administration of respective reagents, mice were anesthetized using 2% pentobarbital sodium (50 mg/kg). Subsequently, a T-shaped incision was carefully made along the median line of the neck to expose the trachea, enabling a thorough evaluation of pulmonary function. A tracheal catheter was then inserted to facilitate the assessment of pulmonary function. After completing functional measurements, mice were immediately euthanized, and lung tissues were harvested for subsequent analyses. The end pulmonary index, a vital metric reflecting pulmonary changes, was calculated using the following formula: pulmonary index = (pulmonary weight (mg)/body weight (g)) × 100%.

2.6. Histological Analysis

After 14 days of daily treatment, mice were humanely euthanized, and left lung tissues were carefully harvested. The harvested tissues were then fixed in 4% formalin for 24 h, followed by systematic dehydration

and paraffin embedding. Subsequently, paraffin-embedded tissues were sliced into 5-μm sections for comprehensive histopathological staining using hematoxylin and eosin (H&E), Sirius Red, Masson's trichrome, and Prussian blue staining following the manufacturer's instructions. The processed tissue sections were dehydrated and sealed with neutral resin. Histopathological changes were examined under an optical microscope (Olympus BX43, Tokyo, Japan) and analyzed with Image Pro Plus 6.0 software. Additionally, the degree of alveolar inflammation and lung damage was assessed using the Szapie scoring criteria: 0 scores, healthy lung tissue; 1 score, mild alveolitis affecting <20% of the total lung area; 2 scores, moderate alveolitis, affecting 20–50% of the total lung area; and 3 scores, severe alveolitis, affecting >50% of the total lung area. The Szapie scoring criteria offered a structured and quantifiable approach to evaluate the extent of alveolar inflammation and lung damage, contributing valuable insights into the pathological changes associated with the experimental conditions [22]. Moreover, the severity of PF was assessed utilizing the Ashcroft scoring criteria, a widely employed system for evaluating histopathological changes. The criteria encompass various scores: 0 scores, healthy lung tissue; 1 score, partial enlargement of the alveoli and slight thickening of the alveolar septum (≤3 times normal); 2 scores, moderate thickening of the alveolar septum (>3 times normal) without lung structural damage; 3 scores, moderate thickening of the alveolar septum (>3 times normal) with increased fibrous pulmonary tissue; 4 scores, the formation of fibrous tissue mass covering <10% of the total lung tissue, accompanied by mild lung structural damage; 5 scores, the area of fibrous tissue mass formation accounting for 10 – 50% of the total lung tissue area, accompanied by lung structural damage; 6 scores, the formation area of fibrous tissue mass covering >50% of the total lung tissue, and significant lung structural damage; 7 scores, severe lung structural damage and a large area of fibrosis, forming a honeycomb lung; and 8 scores, full fibrous lung tissue. This scoring system provides a nuanced and quantitative evaluation of the pathological alterations in lung tissues, enhancing the precision of PF severity assessment [23].

2.7. Immunofluorescence

Tissue sections were initially heated with citrate repair solution for 8 min after dewaxing and hydration. Subsequently, sections were incubated at 4 °C overnight with primary antibodies against α-SMA and Nrf2. Afterward, sections were thoroughly washed with a phosphate-buffered saline (PBS) buffer and subsequently incubated with Alexa Fluor 488-conjugated goat anti-rabbit antibody (1:100) and Alexa Fluor 594-conjugated goat anti-rabbit antibody (1: 100) for 1 h at room temperature, respectively. 4′, 6-diamidino-2-phenylindol (DAPI) stain was applied for 5 min to visualize nuclei. Sections were then coverslipped using an anti-fluorescence attenuation tablet, followed by a systematic examination. At least 6 random microscopic fields were selected under a fluorescence microscope (Olympus BX53, Tokyo, Japan) and the intensity of fluorescence was quantified using Image Pro Plus 6.0.

2.8. Cytokine Measurements

The collected mouse serum and the supernatant obtained from centrifugation of homogenized lung tissue were utilized for subsequent analysis. MDA content and MPO, T-AOC, GSH, and SOD activities were determined using respective colorimetric activity assay kits following the manufacturer's instructions. The absorbance was measured at 460 nm to assess MDA levels and MPO, T-AOC, and SOD activities.

2.9. Western Blot Analysis

Protein expression levels were detected by western blotting as previously described [24]. Briefly, protein samples were extracted from lung tissue and dissolved in radioimmunoprecipitation assay (RIPA) buffer containing 10% proteinase inhibitor phenylmethylsulfonyl fluoride (PMSF) and protein phosphatase inhibitors, respectively. The protein concentration was determined using a BCA protein assay kit. Subsequently, quantitative protein samples from each group were separated by 10% sodium dodecyl sulfate-polyacrylamide gel electrophoresis and then electro-transferred onto nitrocellulose membranes. Afterward, membranes were blocked with 5% skim milk at room temperature for 2 h and then incubated at 4 °C overnight with primary antibodies, including Keap1 (1:1000), HO-1 (1:1000), GPX4 (1:1000), α-SMA (1:

1000), and β-actin (1: 2000). The membranes were subsequently incubated with HRP-labeled secondary antibodies: HRP-conjugated Affinipure Goat Anti-Mouse IgG (1: 5000) or HRP-conjugated Affinipure Goat Anti-Rabbit IgG (1: 5000) at room temperature for 2 h. Finally, membranes were visualized with enhanced chemiluminescence (ECL) reagents and analyzed using a ChemiDoc MP Imaging System (Bio-Rad Laboratories, Inc., Hercules, CA, USA) (Figure S1).

2.10. Statistical Analysis

All data were analyzed using SPSS version 26.0. A one-way analysis of variance (ANOVA) was employed for multiple group comparisons. The homogeneity of variance was tested with $P > 0.05$ using the least significant difference (LSD) method. The Dunnett's T3 method was applied when the homogeneity of variance was not met ($P < 0.05$). Data were presented as mean ± standard error of the mean (SEM). $P < 0.05$ was considered statistically significant.

3. Results

3.1. Effects of G-Re on Body Weight and Lung Index in PF Mice

An animal lung function test system was employed to systematically body weight and lung index in BLM-induced PF mice. The results revealed significant differences between the Sham and the Model groups. Mice in the Model group exhibited signs of lethargy, sluggish movement, substantial weight loss, and an increase in pulmonary index. However, continuous administration of G-Re for 14 days markedly ameliorated these symptoms, leading to a significant decrease in lung index ($P < 0.05$) (Figure 1). These results suggested a positive influence of G-Re in mitigating the physiological consequences of PF, contributing to its potential as a therapeutic strategy for PF.

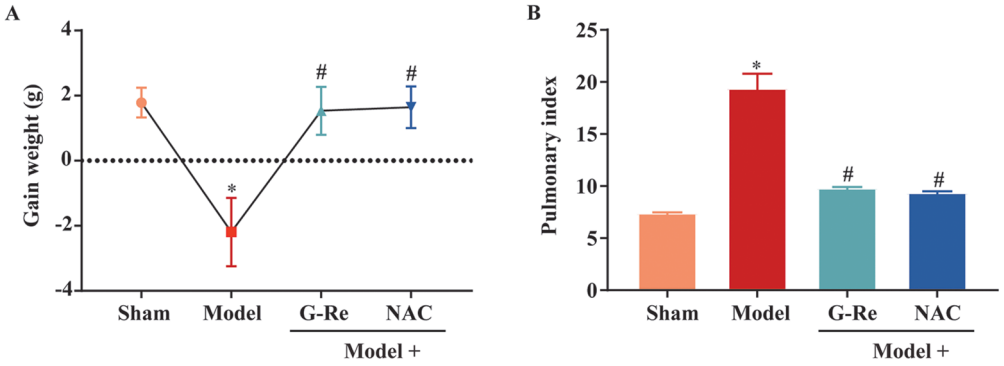

Figure 1. G-Re increased the net body weight and decreased the lung index in BLM-induced PF mice. Mice in Model + G-Re group and Model + NAC group were intragastric administration with G-Re (10 mg/kg) or NAC for 14 days, respectively, while mice in Sham group and Model group were gavaged with the equal volume of normal saline after BLM treatment. (A) The body weight change curve of mice in each group; (B) Pulmonary coefficient of mice in each group. Data are shown as the mean ± SEM (n = 10; * $P < 0.05$ significantly different from the Sham group; $^{\#}$ $P < 0.05$ significantly different from the Model group).

3.2. Effect of G-Re on Pulmonary Function in PF Mice

Functional residual capacity (FRC), forced vital capacity (FVC), maximal mid-expiratory flow curve (MMEF), and inspiratory capacity (IC) were comprehensively assessed using a pulmonometer before the mice were sacrificed to investigate the effect of G-Re on pulmonary function in BLM-induced PF mice. The results revealed a significant reduction in FRC, FVC, MMEF, and IC in PF mice compared with the Sham group. However, continuous administration of G-Re for 14 days significantly improved FRC, FVC, MMEF, and IC in PF mice (Figure 2). These results indicated that G-Re ameliorates BLM-induced pulmonary ventilation disorder in mice, suggesting that G-Re may alleviate the pathological process of PF.

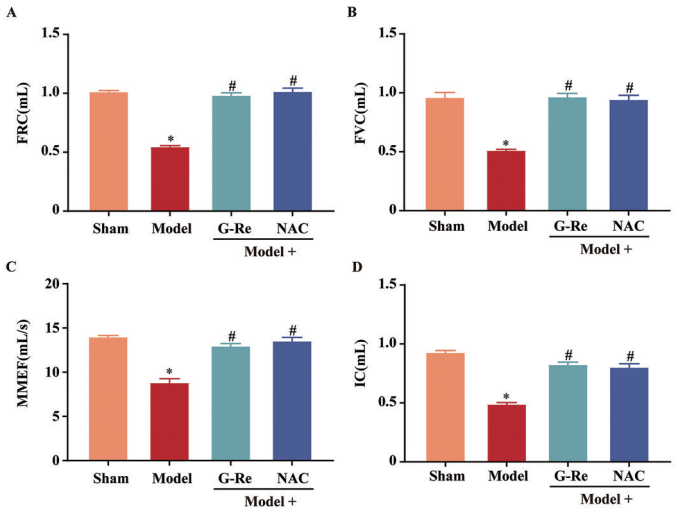

Figure 2. G-Re alleviated lung dysfunction in BLM-induced PF mice. The lung function was measured through a spirometer including (A) FRC, (B) FVC, (C) MMEF, and (D) IC before the mice were sacrificed; Data are presented as the mean ± SEM (n = 6; * $P < 0.05$ significantly different from the Sham group; $^{\#}$ $P < 0.05$ significantly different from the Model group).

3.3. Effect of G-Re on Pulmonary Histopathological Morphology in PF Mice

Histological evaluation using H&E staining was employed to examine pulmonary pathological changes following BLM instillation. H&E staining results revealed disordered pulmonary alveolar structures accompanied by pulmonary interstitial hyperplasia in the Model group. However, these pathological symptoms were markedly alleviated in the Model + G-Re group (Figure 3A). Furthermore, the Szapiel and Ashcroft scoring systems were utilized to quantify alveolar inflammation and PF in mice post-BLM infusion, revealing an exceptionally severe condition compared with the Sham group. Remarkably, the administration of G-Re at a dose of 10 mg/kg mitigated both inflammation and PF lesions on day 14 in PF mice (Figure 3B, C). Collectively, these findings underscore the potential therapeutic efficacy of G-Re in treating BLM-induced PF.

3.4. Effect of G-Re on Collagen Deposition in Lung Tissue of PF Mice

Sirius Red and Masson's trichrome staining were employed histological techniques to examine the effect of G-RE on BLM-induced collagen deposition and PF in mouse lung tissues. Sirius Red staining imparts a red color to collagen fibers, facilitating a visual representation of collagen deposition. Collagen deposition was evident in PF mice, including increased collagen fibers in alveolar septa, around bronchi, and in other structures (Figure 4A). Additionally, Masson's trichrome staining imparts a blue color to collagen and muscle fibers and a red color to the cytoplasm. Results showed clear blue-stained collagen fibers in lung fibrosis mice, indicating a higher prevalence of fibrotic lesions (Figure 4C). Conversely, continuous treatment with G-Re for 14 days significantly ameliorated these structural changes, including a significant reduction in collagen deposition and fibrotic lesions in the lung tissues of PF mice, further confirmed by the corresponding collagen volume fraction (Figure 4B, D). The observed reduction in collagen deposition and fibrotic lesions with G-Re treatment suggests its potential as a therapeutic intervention in mitigating BLM-induced PF.

3.5. Effect of G-Re on α-SMA in PF Mice

α-SMA is a hallmark protein indicating the activity of pulmonary myofibroblasts, and its expression level is closely associated with collagen protein deposition. Hence, immunofluorescence was performed to examine α-SMA protein expression in mouse lung tissue to further investigate the protective effects of G-Re against BLM-induced PF in mice. Compared with the Sham group, the Model group showed increased fluorescence intensity of α-SMA protein, signifying elevated levels after BLM instillation. Conversely, the Model + G-Re group displayed a significant reduction in α-SMA protein levels compared with the Model group (Figure 5). These results indicated that G-Re can mitigate collagen deposition in the lungs of PF mice.

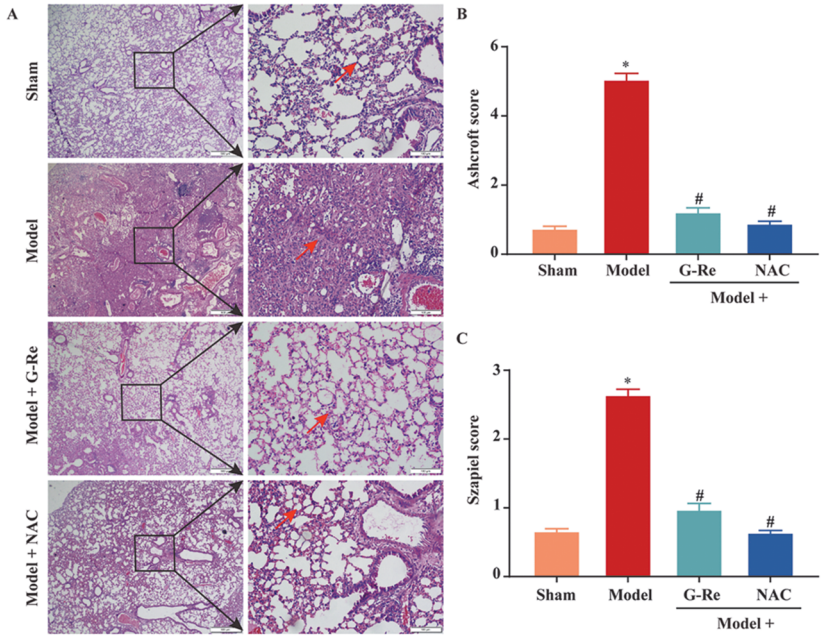

Figure 3. G-Re ameliorated pulmonary injury in BLM-induced PF mice. Successful establishment of BLM-induced acute lung injury in *vivo*. The mice were anesthetized with 2% pentobarbital sodium (50 mg/kg) and then BLM was injected into the trachea followed by gavage with G-Re or NAC for 14 days, continuously. (A) Representative images of H&E staining in Sham, Model, Model + G - Re, and Model + NAC groups. The red arrows indicate the damaged alveolar structure. Scale bar = 500 μm, 4×; 100 μm, 20×; (B) Ashcroft score of lung tissue; (C) Szapiel score of lung tissue. Data are shown as the mean ± SEM (n = 6; * $P < 0.05$ significantly different from the Sham group; $^{\#}$ $P < 0.05$ significantly different from the Model group).

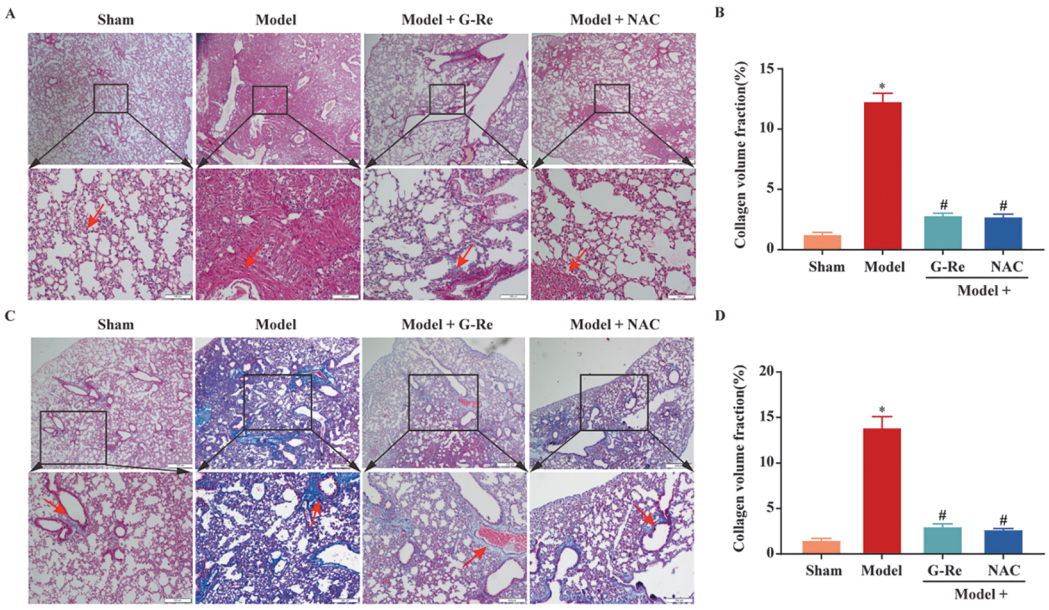

Figure 4. G-Re attenuated lung collagen deposition and lung fibrosis in BLM-induced PF mice. The mouse lung tissue was collected after BLM instillation followed by gavage G-Re for 14 days. (A) Representative images of the Sirius red staining (pink) in Sham, Model, Model + G - Re, and Model + NAC groups. The red arrows point to areas with significant collagen deposition, scale bar = 500 μm, 4×; 100 μm, 20×. (B) Area density analysis of Sirius red staining; (C) Representative images of the Masson staining assay (blue) in Sham, Model, Model + G - Re, and Model + NAC groups. The red arrows represent the collagen volume fraction among different groups, scale bar = 500 μm, 4×; 100 μm, 20×. (D) Area density analysis of Masson staining Data are shown as the mean ± SEM (n = 6; * $P < 0.05$ significantly different from the Sham group; $^{\#}$ $P < 0.05$ significantly different from the Model group).

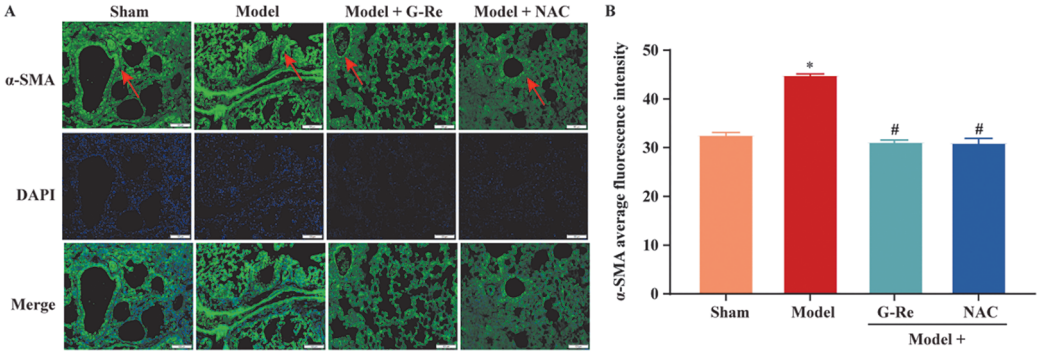

Figure 5. G-Re reduced α-SMA protein level in lung tissue of BLM-induced PF mice. The mouse lung tissue was collected after BLM instillation followed by gavage G-Re for 14 days. (A) Immunofluorescence staining of α - SMA (green), DAPI (blue), and their merge in Sham, Model, Model + G - Re, and Model + NAC groups. The red arrows indicate protein deposits in different groups, scale bar = 100 μm, 20× ; (B) The analysis of α -SMA average fluorescence intensity among different groups; Data are presented as the mean ± SEM (n = 6; * $P < 0.05$ significantly different from the Sham group; $^{\#}$ $P < 0.05$ significantly different from the Model group).

3.6. Effect of G-Re on Oxidative Stress-Related Indicators in PF Mice

Oxidative stress is implicated in the pathogenesis of PF. Therefore, we initially assessed oxidative markers, including MDA, MPO, T-AOC, GSH, and SOD. It was found that MDA content and MPO activity were significantly increased and T-AOC and GSH activities were markedly decreased in PF mice (Figure 6A–F). Additionally, the suppression rate of SOD was dramatically enhanced, with a significant decrease in its activity. However, all these effects were reversed by G-Re treatment (10 mg/kg). Taken together, these data suggest that G-Re can alleviate BLM-induced oxidative stress injury in PF mice.

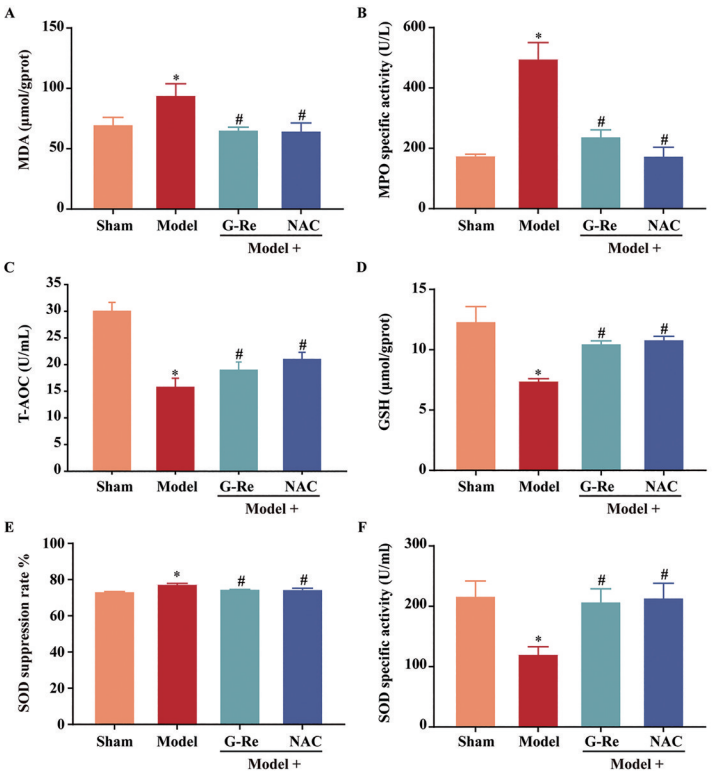

Figure 6. G-Re regulated oxidative stress-related indicators including MDA, MPO, T-AOC, GSH, SOD in serum by colorimetric preparation kit and statistical analysis. (A) MDA content; (B) MPO activity; (C) T-AOC content; (D) GSH content; (E) SOD suppression rate; (F) SOD activity. Data are presented as the mean ± SEM (n = 6; * $P < 0.05$ significantly different from the Sham group; $^{\#}$ $P < 0.05$ significantly different from the Model group).

3.7. Effect of G-Re on Nrf2 Nuclear Translocation in PF Mice

Given the pivotal role of oxidative stress in the physiological and pathological processes of PF, we employed immunofluorescence staining to assess the nuclear translocation of Nrf2, a key nuclear transcription factor in oxidative stress regulation. Red fluorescence in immunofluorescence images represents Nrf2 expression, whereas blue fluorescence corresponds to the nucleus when using DAPI. As depicted in Figure 7A, Nrf2 nuclear translocation was significantly reduced in the lung tissue of Model compared with Sham mice. The Pearson correlation coefficient was also significantly decreased, further confirming a notable reduction in Nrf2 nuclear translocation in the Model group. Conversely, the expression of nuclear red fluorescence was significantly increased in the lung tissue of Model + G-Re compared with Model mice. The Pearson correlation coefficient was also significantly increased. The observed enhancement of Nrf2 nuclear translocation by G-Re highlights its potential as a therapeutic agent against oxidative stress in PF, and further understanding of Nrf2-mediated pathways may provide insights for targeted PF therapies.

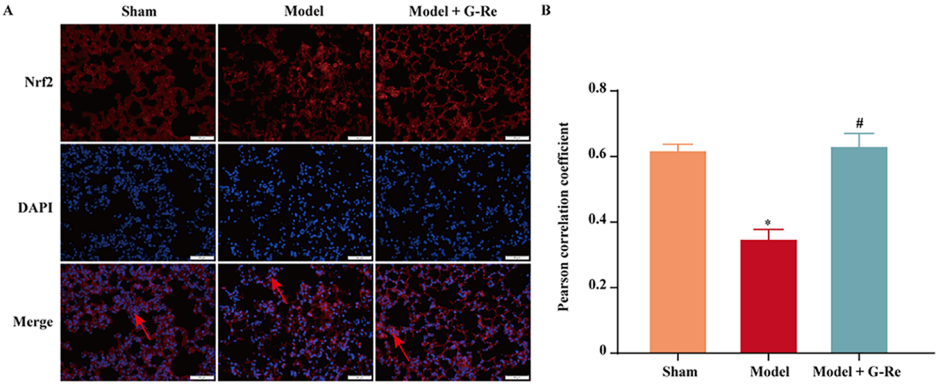

Figure 7. G-Re promoted Nrf2 nuclear translocation in BLM-induced PF mice. (A) Immunofluorescence staining of Nrf2 (red), DAPI (blue), and their merge in Sham, Model, and Model + G - Re groups. The red arrows indicate Nrf2 translocation from cytoplasm to the nucleus, Scale bar = 100 μm, 20×; (B) Pearson correlation coefficient among different groups. Data are the presented as the mean ± SEM (n = 6; * $P < 0.05$ significantly different from the Sham group; $^{\#}$ $P < 0.05$ significantly different from the Model group).

3.8. Effect of G-Re on Keap-1, HO-1, and NQO-1 Protein Expression in PF Mice

Next, the expression of Nrf2-related proteins, including Keap-1, HO-1, and NQO-1 was assessed by western blot analysis to further explore the potential involvement of the Nrf2 signaling pathway in BLM-induced PF in mice. As depicted in Figure 8, the results revealed significant alterations in protein expression in the Model group compared with the Sham group. Specifically, Keap1 protein expression was significantly upregulated and HO-1 and NQO-1 protein expressions were significantly down-regulated in the Model group, which were significantly reversed by G-Re (10 mg/kg) treatment (Figure 8A – D). These findings highlight the potential role of the Nrf2 signaling pathway in the development of BLM-induced PF and the regulatory effects of G-Re on Keap-1, HO-1, and NQO-1 protein expressions.

3.9. Effect of G-Re on GPX4 Protein Expression and Iron Ion Deposition in Lung Tissues of PF Mice

Furthermore, the expression of molecules associated with ferroptosis was assessed to investigate the potential mechanism by which G-Re alleviates BLM-induced PF in mice. Prussian blue staining results provided insight into iron concentrations. Notably, the Model group exhibited an increase in iron levels, indicative of a perturbation in iron homeostasis. In contrast, the Model + G-Re group displayed relatively normal iron levels compared with the Sham group (Figure 9A,B). The protein expression of GPX4, a pivotal protein in the regulation of ferroptosis, was also examined. The Model group exhibited lower GPX4 expression than the Sham group. Conversely, mice in the Model + G-Re group exhibited higher GPX4 levels than those treated with BLM alone, indicating that G-Re effectively inhibited BLM-induced ferroptosis in PF mice. These findings suggested a potential role for G-Re in modulating ferroptosis, a form of regulated cell death associated with iron-dependent lipid peroxidation, in PF mice.

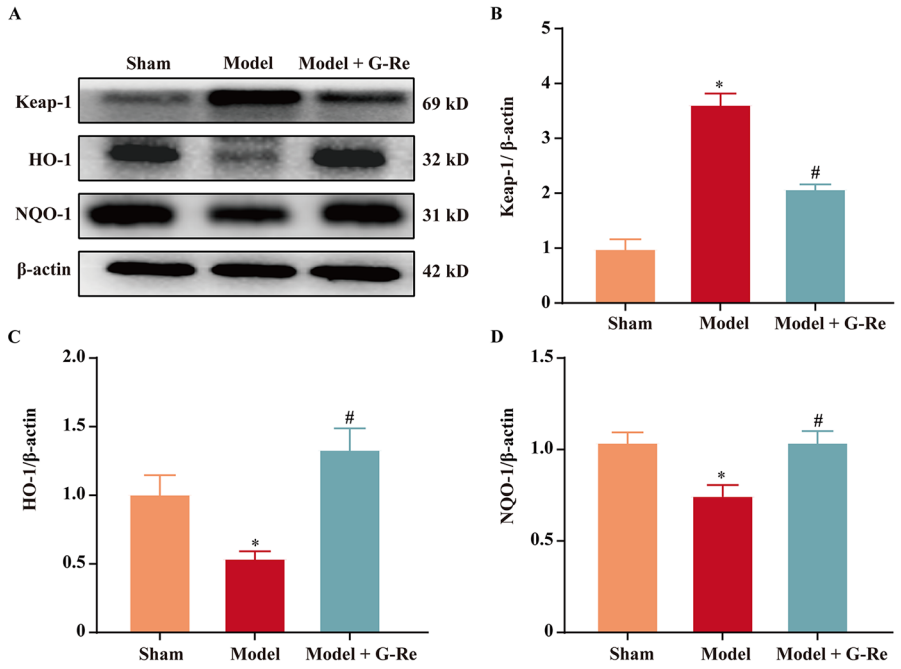

Figure 8. G-Re relieved oxidative stress injury by regulating the Nrf2/Keap1 signaling pathway in BLM-induced PF mice. (A) Representative images of western blot for Keap1, HO-1, NQO-1protein expressions, respectively. β-actin was applied as loading control; (B) Quantitative analysis of Keap1 protein expression (n = 5); (C) Quantitative analysis of HO-1 protein expression (n = 5); (D) Quantitative analysis of NQO-1 protein expression (n = 5). Data are presented as the mean ± SEM (n = 6; * $P < 0.05$ significantly different from the Sham group; # $P < 0.05$ significantly different from the Model group).

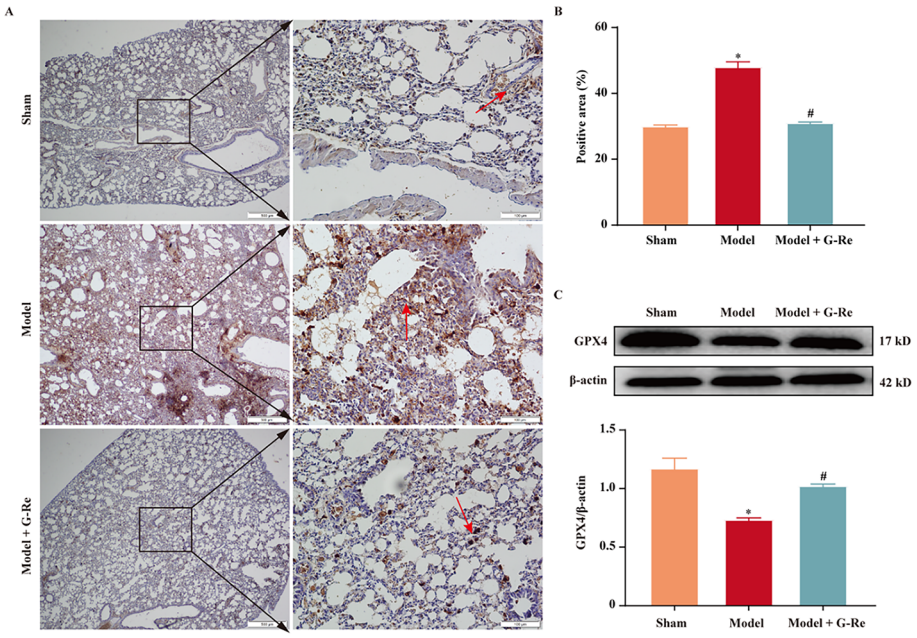

Figure 9. G-Re effectively inhibited the ion deposition and GPX4 protein expression in BLM-induced PF mice. (A) Representative images of mouse lung tissue stained with Prussian blue in Sham, Model, and Model + G - Re groups. The red arrows indicate regions with notable Prussian blue staining, suggesting areas of iron accumulation or relevant pathological features, scale bar = 500 μm, 4×; 100 μm, 20×; (B) Quantitative analysis of iron deposit positive area in each group; (C) Representative image and quantitative analysis of western blot for GPX4 protein expression. β-actin was applied as loading control; *Data are presented the mean ± SEM (n = 6; * $P < 0.05$ significantly different from the Sham group; # $P < 0.05$ significantly different from the Model group).

4. Discussion

The present study has for the first time demonstrated that G-Re effectively alleviates BLM-induced PF in mice. The potential molecular mechanism may be linked to its anti-oxidative stress effects through the activation of the Nrf2/Keap1 signaling pathway. Notably, the reduction in iron sedimentation and GPX4 protein expression suggests the involvement of cell ferroptosis in the protective action of G-Re against PF injury. Overall, these findings highlight that G-Re exerts a protective role by modulating the Nrf2/Keap1/GPX4 axis, providing a pharmacological foundation for developing PF treatment strategies that warrant further exploration.

BLM has been widely used to investigate the mechanism of PF in mice, which induces inflammatory cell infiltration, fibrosis, and pulmonary structure disorders, resulting in restricted dyspnea and ventilation dysfunction [25]. The current study showed that body weight gain was significantly decreased and the lung coefficient was remarkably increased after BLM instillation. Moreover, the pulmonary dysfunction significantly worsened 14 days post-BLM exposure, evidenced by the reduced FVC, FRC, MMEF, and IC [26]. Notably, G-Re effectively mitigated these effects after BLM treatment. Similarly, H&E staining results further confirmed that G-Re reversed the pathological morphology of lung tissue in PF mice, evidenced by increased inflammatory cell infiltration, alveolar structure disorder, and lung tissue destruction after BLM instillation. These results affirm the inhibitory role of G-Re in the pathological progression of PF.

Numerous clinical and experimental studies have demonstrated that the pathological process of PF is closely associated with sustained damage to the alveolar epithelium, triggering downstream effector cell recruitment and fibrotic factor secretion. Among them, the released pro-fibrotic factors initiate epithelial-mesenchymal transformation and fibroblast-to-myofibroblast transdifferentiation, which is a key driver promoting PF formation [27]. Particularly, myofibroblasts, key contributors to PF, deposit excessive extracellular matrix components and resist apoptosis, leading to abnormal fibrous tissue formation. Moreover, α-SMA is a signature protein of lung myoblast activity, and its expression level can directly reflect the situation of collagen deposition [28]. The present study found that G-Re inhibited collagen deposition and lung fibrosis in PF mice, as evidenced by Sirius Red and Masson's trichrome staining. Furthermore, G-Re reduced α-SMA levels in the lung tissue of PF mice, demonstrating its ability to mitigate BLM-induced collagen deposition.

Previous studies have shown that the pathological progression of PF is closely associated with oxidative stress damage. Therefore, MDA and MPO, markers of oxidative stress injury, were measured to determine whether oxidative stress is a key factor in BLM-induced PF [29, 30]. Our findings showed that G-Re significantly reduced lung tissue MDA levels and serum MPO activity in PF mice, suggesting that G-RE may play a potential role in mitigating lipid peroxidation induced by excessive ROS accumulation. NAC, a well-known antioxidant that scavenges free radicals and boosts GSH synthesis, is widely used in clinical respiratory disease treatment. NAC, widely used to study oxidative stress injuries, served as a positive control in the current study [31, 32]. In our previous study of redox homeostasis maintenance, we discovered that Nrf2, a key redox transcription factor, plays a crucial role in balancing oxidation and antioxidant capacity. Nrf2 remains bound to Keap1 in the cytoplasm with low activity under normal physiological conditions. However, Nrf2 dissociates from Keap1 and translocates into the nucleus after exposure to oxidative stress, where it binds to antioxidant response elements (ARE), initiating the transcription and expression of downstream antioxidant enzymes (e.g., GPX4 and SOD) and phase II detoxification enzymes (e.g., HO-1 and NQO-1) [33]. This cascade enhances cellular T-AOC and preserves cell redox homeostasis. The present study found that G-Re promoted Nrf2 nucleation in the lung tissue of PF mice. Concurrently, G-Re inhibited the expression of Keap1 protein and upregulated the expression levels of HO-1 and NQO-1 proteins. Importantly, G-Re also increased SOD, T-AOC, and GSH activities in the lung tissue of PF mice. These findings suggest that G-Re can mitigate BLM-induced PF in mice by activating the Nrf2/Keap1 signaling pathway.

Our study also discovered that G-Re significantly reduced the protein expression of GPX4 in the lung tissue of PF mice. GPX4 is a central regulatory factor in ferroptosis, and its decline is regarded as a hallmark of ferroptosis [34]. Ferroptosis represents an iron-dependent form of regulated cell death characterized by the toxic accumulation of lipid peroxides on the cell membrane, which is closely associated with oxidative stress [35]. Based on this discovery, it has also been recognized that ferroptosis plays a crucial role in the

progression of PF, and its potential molecular mechanisms are increasingly being unveiled [36, 37]. The current study revealed that G-Re significantly reduced protein expression of GPX4 in the lung tissue of PF mice, suggesting that the alleviating effect of G-Re on PF may involve ferroptosis. The results of Prussian blue staining further validated this conclusion, indicating that G-Re has a mitigating effect on iron ion precipitation in the lung tissue of PF mice.

In summary, this study preliminarily investigated the impact of G-Re on BLM-induced PF in mice, primarily focusing on oxidative stress damage. The findings demonstrated that continuous administration of G-Re at a dosage of 10 mg/kg effectively reduced lung tissue injury and enhanced the antioxidant capacity in PF mice. Moreover, the study identified a correlation between the protective effect of G-Re against BLM-induced PF in mice and the activation of the Nrf2/Keap1 signaling pathway and ferroptosis. However, the specific molecular mechanisms have not been thoroughly investigated. T further exploration of potential mechanisms can be pursued using protein inhibitors, gene knockout techniques, network pharmacology, and other methodologies in subsequent studies (Figure 10).

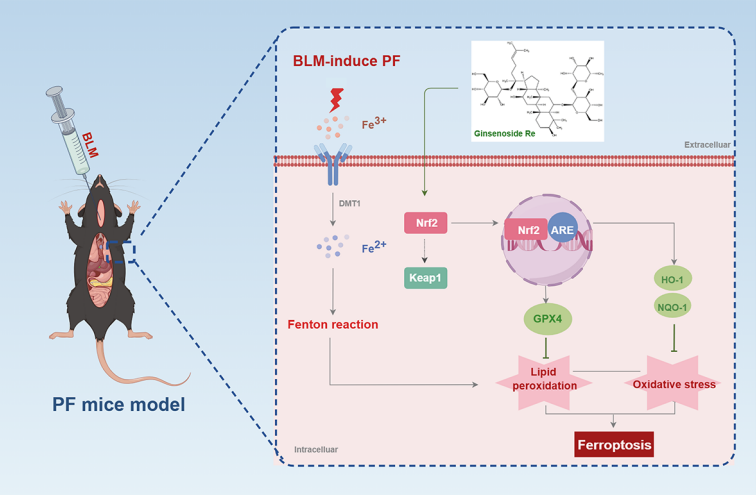

Figure 10. Schematic diagram showing the mechanism by which G-Re alleviates BLM-induced PF injury by inhibiting the Nrf2/Keap1/GPX4 axis in mice.

Supplementary Materials: The following supporting information can be downloaded at: https://www.sciltp.com/journals/ijddp/2024/4/662/s1, Figure S1: The original western blot membrane.

Author Contributions: In this research endeavor, the contributions of all participants are as follows: H. L.: conceptualization, methodology, software; L. F., H. L.: data curation, writing—original draft preparation; H. L.: visualization, investigation; X.C., Y.S.: supervision; Z.W.: software, validation; J.D.: writing—reviewing and editing. All authors have read and agreed to the published version of the manuscript.

Funding: This study was supported by the National Natural Science Foundation of China (Grant nos. 81860732).

Institutional Review Board Statement: The study was conducted according to the guidelines of the Declaration of Helsinki, and approved by the Ethics Committee of Zunyi Medical University (Guizhou, China, No. ZMU21-2203-583), the ethical approval number is ZMU11-2203-357 and the approval date is March 7, 2022.

Informed Consent Statement: Not applicable.

Data Availability Statement: Not applicable.

Conflicts of Interest: The authors declare that there are no conflicts of interest.

References

1. Chanda, D.; Otoupalova, E.; Smith, S.R.; et al. Developmental Pathways in the Pathogenesis of Lung Fibrosis. *Mol. Asp. Med.* **2019**, *65*, 56–69. https://doi.org/10.1016/j.mam.2018.08.004
2. Spagnolo, P.; Kropski, J. A.; Jones, M. G.; et al. Idiopathic PF: Disease Mechanisms and Drug Development. *Pharmacol. Ther.* **2021**, *222*, 107798. https://doi.org/10.1016/j.pharmthera.2020.107798.
3. Albert, R.K.; Phimister, E.G.; Schwartz, D.A. Revealing the Secrets of Idiopathic PF. *N. Engl. J. Med.* **2019**, *380*, 94–96. https://doi.org/10.1056/NEJMcibr1811639.
4. Baradaran, H. R.; Jiang, C.; Huang, H.; et al. Adverse Events of Pirfenidone for the Treatment of PF: A Meta-Analysis of Randomized Controlled Trials. *PLoS ONE* **2012**, *7*, e47024. https://doi. org/10.1371/journal. pone. 0047024.

5. Flaherty, K.R.; Wells, A.U.; Cottin, V.; et al. Nintedanib in Progressive Fibrosing Interstitial Lung Diseases. *New Engl. J. Med.* **2019**, *381*, 1718–1727. https://doi.org/10.1056/NEJMoa1908681.
6. Fois, A. G.; Paliogiannis, P.; Sotgia, S.; et al. Evaluation of Oxidative Stress Biomarkers in Idiopathic PF and Therapeutic Applications: A Systematic Review. *Respir. Res.* **2018**, *19*, 51. https://doi. org/10.1186/s12931-018-0754-7.
7. Otoupalova, E.; Smith, S.; Cheng, G.; et al. Oxidative Stress in PF. *Compr. Physiology.* **2020**, *10*, 509–547.
8. Feng, L.; Gao, J.; Liu, Y.; et al. Icariside Ii Alleviates Oxygen-Glucose Deprivation and Reoxygenation-Induced Pc12 Cell Oxidative Injury by Activating Nrf2/Sirt3 Signaling Pathway. *Biomed. Pharmacother.* **2018**, *103*, 9–17. https://doi.org/10.1016/j.biopha.2018.04.005.
9. Kudryavtseva, A.V.; Krasnov, G.S.; Dmitriev, A.A.; et al. Mitochondrial Dysfunction and Oxidative Stress in Aging and Cancer. *Oncotarget* **2016**, *7*, 44879–44905.
10. Liu, J.; Wu, Z.; Liu, Y.; et al. Ros-Responsive Liposomes as an Inhaled Drug Delivery Nanoplatform for Idiopathic PF Treatment Via Nrf2 Signaling. *J. Nanobiotechnol.* **2022**, *20*, 213. https://doi.org/10.1186/s12951-022-01435-4.
11. Zeng, Q.; Zhou, T.; Zhao, F.; et al. P62-Nrf2 Regulatory Loop Mediates the Anti-PF Effect of Bergenin. *Antioxidants* **2022**, *11*, 307. https://doi.org/10.3390/antiox11020307.
12. Jiang, X.; Stockwell, B.R.; Conrad, M. Ferroptosis: Mechanisms, Biology and Role in Disease. *Nat. Rev. Mol. Cell Biol.* **2021**, *22*, 266–282. https://doi.org/10.1038/s41580-020-00324-8.
13. He, R.; Liu, B.; Xiong, R.; et al. Itaconate Inhibits Ferroptosis of Macrophage Via Nrf2 Pathways against Sepsis-Induced Acute Lung Injury. *Cell Death Discov.* **2022**, *8*, 43. https://doi.org/10.1038/s41420-021-00807-3.
14. Imai, H.; Matsuoka, M.; Kumagai, T.; et al. Lipid Peroxidation-Dependent Cell Death Regulated by Gpx4 and Ferroptosis. In *Apoptotic and Non-Apoptotic Cell Death*; Springer: Cham, Switzerland; 2016, Vol. 403, pp. 143–170.
15. El-Horany, H.E.-S.; Atef, M.M.; Abdel Ghafar, M.T.; et al. Empagliflozin Ameliorates Bleomycin-Induced PF in Rats by Modulating Sesn2/Ampk/Nrf2 Signaling and Targeting Ferroptosis and Autophagy. *Int. J. Mol. Sci.* **2023**, *24*, 9481. https://doi.org/10.3390/ijms24119481.
16. Wang, Y.; Wei, J.; Deng, H.; et al. The Role of Nrf2 in PF: Molecular Mechanisms and Treatment Approaches. *Antioxidants* **2022**, *11*, 1685. https://doi.org/10.3390/antiox11091685.
17. Mancuso, C.; Santangelo, R. Panax Ginseng and Panax Quinquefolius: From Pharmacology to Toxicology. *Food Chem. Toxicol.* **2017**, *107*, 362–372. https://doi.org/10.1016/j.fct.2017.07.019.
18. Wang, Q.-W.; Yu, X.-F.; Xu, H.-L.; et al. Ginsenoside Re Attenuates Isoproterenol-Induced Myocardial Injury in Rats. *Evid. -Based Complement. Altern. Med.* **2018**, *2018*, 8637134. https://doi.org/10.1155/2018/8637134.
19. Madhi, I.; Kim, J. -H.; Shin, J. E.; et al. Ginsenoside Re Exhibits Neuroprotective Effects by Inhibiting Neuroinflammation Via Camk/Mapk/Nf-Kb Signaling in Microglia. *Mol. Med. Rep.* **2021**, *24*, 698. https://doi.org/10.3892/mmr.2021.12337.
20. Gao, X.-Y.; Liu, G.-C.; Zhang, J.-X.; et al. Pharmacological Properties of Ginsenoside Re. *Front. Pharmacol.* **2022**, *13*, 754191. https://doi.org/10.3389/fphar.2022.754191.
21. Calverley, P.; Rogliani, P.; Papi, A. Safety of N-Acetylcysteine at High Doses in Chronic Respiratory Diseases: A Review. *Drug Saf.* **2020**, *44*, 273–290. https://doi.org/10.1007/s40264-020-01026-y.
22. Szapiel, S.V.; Elson, N.A.; Fulmer, J.D.; et al. Bleomycin-Induced Interstitial Pulmonary Disease in the Nude, Athymic Mouse. *Am. Rev. Respir. Dis.* **1979**, *120*, 893–899.
23. Ashcroft, T.; Simpson, J.M.; Timbrell, V. Simple Method of Estimating Severity of PF on a Numerical Scale. *J. Clin. Pathol.* **1988**, *41*, 467–470.
24. Feng, L.; Li, Y.; Lin, M.; et al. Trilobatin Attenuates Cerebral Ischaemia/Reperfusion-Induced Blood–Brain Barrier Dysfunction by Targeting Matrix Metalloproteinase 9: The Legend of a Food Additive. *Br. J. Pharmacol.* **2023**, *181*, 1005–1027. https://doi.org/10.1111/bph.16239.
25. Kolb, P.; Upagupta, C.; Vierhout, M.; et al. The Importance of Interventional Timing in the Bleomycin Model of PF. *Eur. Respir. J.* **2020**, *55*, 1901105. https://doi.org/10.1183/13993003.01105-2019.
26. Nathan, S.D.; Wanger, J.; Zibrak, J.D.; et al. Using Forced Vital Capacity (Fvc) in the Clinic to Monitor Patients with Idiopathic PF (Ipf): Pros and Cons. *Expert Rev. Respir. Med.* **2020**, *15*, 175–181. https://doi.org/10.1080/17476348.2020.1816831.
27. Wang, Y.C.; Xie, H.; Zhang, Y.C.; et al. Exosomal Mir-107 Antagonizes Profibrotic Phenotypes of Pericytes by Targeting a Pathway Involving Hif-1α/Notch1/Pdgfrβ/Yap1/Twist1 Axis in Vitro. American journal of physiology. *Heart Circ. Physiol.* **2021**, *320*, H520–H534.
28. Tang, Y.; Yuan, Q.; Zhao, C.; et al. Targeting Usp11 May Alleviate Radiation-Induced PF by Regulating Endothelium Tight Junction. *Int. J. Radiat. Biol.* **2021**, *981*, 30–40. https://doi.org/10.1080/09553002.2022.1998711.
29. Zhao, S.; Zuo, W.; Chen, H.; et al. Effects of Pilose Antler Peptide on Bleomycin-Induced PF in Mice. *Biomed. Pharmacother.* **2019**, *109*, 2078–2083. https://doi.org/10.1016/j.biopha.2018.08.114.
30. Zhou, J.; Peng, Z.; Wang, J. Trelagliptin Alleviates Lipopolysaccharide (Lps)-Induced Inflammation and Oxidative Stress in Acute Lung Injury Mice. *Inflammation* **2021**, *44*, 1507–1517. https://doi.org/10.1007/s10753-021-01435-w.
31. Raghu, G.; Berk, M.; Campochiaro, P.A.; et al. The Multifaceted Therapeutic Role of N-Acetylcysteine (Nac) in Disorders Characterized by Oxidative Stress. *Curr. Neuropharmacol.* **2021**, *19*, 1202–1224. https://doi.org/10.2174/1570159x19666201230144109.
32. Schwalfenberg, G.K.; Emanuelli, T. N-Acetylcysteine: A Review of Clinical Usefulness (an Old Drug with New Tricks). *J. Nutr. Metab.* **2021**, *2021*, *9949453*. https://doi.org/10.1155/2021/9949453.
33. Wang, X.; Wang, Y.; Huang, D.; et al. Astragaloside Iv Regulates the Ferroptosis Signaling Pathway Via the Nrf2/

Slc7a11/Gpx4 Axis to Inhibit Pm2.5-Mediated Lung Injury in Mice. *Int. Immunopharmacol.* **2022**, *112*, 109186. https://doi.org/10.1016/j.intimp.2022.109186.
34. Fan, R.; Sui, J.; Dong, X.; et al. Wedelolactone Alleviates Acute Pancreatitis and Associated Lung Injury Via Gpx4 Mediated Suppression of Pyroptosis and Ferroptosis. *Free Radic. Biol. Med.* **2021**, *173*, 29–40. https://doi.org/10.1016/j.freeradbiomed.2021.07.009.
35. Liu, P.; Feng, Y.; Li, H.; et al. Ferrostatin-1 Alleviates Lipopolysaccharide-Induced Acute Lung Injury Via Inhibiting Ferroptosis. *Cell. Mol. Biol. Lett.* **2020**, *25*, 10. https://doi.org/10.1186/s11658-020-00205-0.
36. Wang, C.; Hua, S.; Song, L. Ferroptosis in PF: An Emerging Therapeutic Target. *Front. Physiol.* **2023**, *14*, 1205771. https://doi.org/10.3389/fphys.2023.1205771.
37. Li, X.; Duan, L.; Yuan, S.; et al. Ferroptosis Inhibitor Alleviates Radiation-Induced Lung Fibrosis (Rilf) Via Down-Regulation of Tgf-B1. *J. Inflamm.* **2019**, *16*, 11. https://doi.org/10.1186/s12950-019-0216-0.